Immunity
Article

Intrinsic Properties of immunoglobulin IgG1 Isotype-Switched B Cell Receptors Promote Microclustering and the Initiation of Signaling

Wanli Liu,[1] Tobias Meckel,[2] Pavel Tolar,[3] Hae Won Sohn,[1] and Susan K. Pierce[1,*]
[1]Laboratory of Immunogenetics, National Institute of Allergy and Infectious Diseases, NIH, Rockville, MD 20852, USA
[2]Darmstadt University of Technology, Department of Biology Membrane Biophysics, Schnittspahnstrasse 3-5, D-64287 Darmstadt, Germany
[3]National Institute for Medical Research, The Ridgeway, Mill Hill, London NW7 1AA, UK
*Correspondence: spierce@nih.gov
DOI 10.1016/j.immuni.2010.06.006

SUMMARY

Memory B cells express high-affinity, immunoglobulin GB cell receptors (IgG BCRs) that enhance B cell responses, giving rise to the rapid production of high-affinity, IgG antibodies. Despite the central role of IgG BCRs in memory responses, the mechanisms by which the IgG BCRs function to enhance B cell responses are not fully understood. Using high-resolution live-cell imaging, we showed that IgG1 BCRs dramatically enhanced the earliest BCR-intrinsic events that followed within seconds of B cells' encounter with membrane bound antigen, including BCR oligomerization and BCR microcluster growth, leading to Syk kinase recruitment and calcium responses. The enhancement of these early events was dependent on a membrane proximal region of the IgG1 cytoplasmic tail not previously appreciated to play a role in IgG1 BCR signaling. Thus, intrinsic properties of the IgG1 BCR enhance early antigen-driven events that ultimately translate into heightened signaling.

INTRODUCTION

Antibody memory, a hallmark of adaptive immunity, is characterized by rapid, high-affinity recall responses that are dominated by IgG antibodies. Antibody memory is encoded in part in memory B cells (MBCs) expressing B cell receptors (BCRs) that contain isotype switched, somatically hypermutated membrane IgGs (mIgGs) in contrast to naive B cells that express BCRs composed of mIgM and mIgD (McHeyzer-Williams and McHeyzer-Williams, 2005). Because all mIgs in BCRs are associated with identical Igα and Igβ heterodimers that connect the antigen-engaged BCR to the B cell's signaling apparatus (Reth, 1992), it has long been suspected that inherent differences in the structures of mIgM and mIgD versus mIgG account for the accelerated and elevated antibody responses of MBCs expressing IgG BCRs compared to naive B cells expressing IgM and IgD BCRs. Both mIgM and mIgD have short, three amino acid cytoplasmic tails that have not been implicated to play a direct role in BCR signaling. In contrast, all mIgG subtypes have highly conserved cytoplasmic domains of 28 residues that are both necessary and sufficient for high-titered IgG memory antibody responses in vivo (Kaisho et al., 1997; Martin and Goodnow, 2002). The mIgG tail has been shown to enhance calcium responses (Horikawa et al., 2007; Waisman et al., 2007; Wakabayashi et al., 2002), possibly through mechanisms that involve CD22 (Wakabayashi et al., 2002), although for a role of CD22 in regulating the rapid kinetics and magnitude of early IgG BCR signaling is controversial (Horikawa et al., 2007; Waisman et al., 2007). Horikawa et al. (2007) showed that the gene transcription profiles activated by IgG BCRs versus IgM BCRs are qualitatively different with the majority of IgM BCR antigen-induced gene expression diminished in antigen-stimulated IgG BCR-expressing B cells, resulting in decreased expression of genes that oppose plasma cell differentiation. Waisman et al. (2007) provided evidence that mIgG can mediate a unique signaling function that, in part, replaces the need for the Igα and Igβ heterodimer, at least during development. A molecular mechanism as to how qualitative differences in IgM and IgG BCRs downstream signaling could be achieved was recently provided by Engels et al. (2009), who showed that a conserved tyrosine in the cytoplasmic domain of the mIgG was phosphorylated upon IgG BCR crosslinking. The phosphorylated tyrosine recruited the adaptor, Grb2, to the IgG BCR, resulting in enhanced calcium response and B cell proliferation.

Studies to elucidate the differences in IgM BCR versus IgG BCR signaling functions have focused thus far on the differences in downstream signaling pathways, leaving unexplored the possible contribution of the mIgG in the early BCR intrinsic events in the initiation of BCR signaling that are upstream of the recruitment of the first kinase in the BCR signaling cascade. Batista and colleagues first showed that when B cells encounter antigen in fluid lipid bilayers, mimicking an antigen-presenting cell, the BCRs form microclusters at the first points of contact of the B cell with the antigen-containing membrane (Fleire et al., 2006). Most recently, this group addressed the steady-state dynamics of the BCR in the absence of antigen and showed that the diffusion of the BCR was restricted by the cytoskeleton and that this restriction likely played a role in controlling BCR signaling possibly related to tonic signaling (Treanor et al., 2010). We have focused on the BCR intrinsic antigen-driven events that lead up to the formation of the BCR microclusters using advanced total internal reflection fluorescence (TIRF)

single-molecule imaging technologies (Tolar et al., 2008, 2009a, 2009b; Tolar and Pierce, 2009, 2010). We provided evidence that BCR oligomerization and microclustering did not require the physical crosslinking of BCRs by antigen but, rather, are driven by BCRs binding to monovalent antigens in fluid lipid bilayers by a mechanism that required antigen binding-induced changes in the IgM BCR's mIg Cμ4 or the IgG1 BCR's Cγ3 membrane proximal domains of the mIg ectodomains (Tolar et al., 2009a). These events were BCR intrinsic and occurred following antigen binding, even in BCRs that were signaling incompetent. We also used TIRF and confocal microscopy in combination with fluorescence resonance energy transfer (FRET) to provide evidence that once clustered by antigen, the BCR's cytoplasmic domains underwent a conformational change from a "closed" to an "open" form (Tolar et al., 2005) that was coincident with a transient perturbation of the local lipid environment and the recruitment of Lyn kinase (Sohn et al., 2008).

Here, we compare these early events for B cells expressing either IgM BCRs or IgG1 BCRs and provide evidence that intrinsic properties of IgG1 BCR cytoplasmic domains promote oligomerization, microclustering, and the initiation of signaling.

RESULTS

IgG1 BCRs Show an Enhanced Ability to Oligomerize

To determine the impact of the expression of mIgG1 versus mIgM on the antigen-driven formation of immobile BCR oligomers (Tolar et al., 2009a; Tolar and Pierce, 2010) independently of the affinity of BCRs for antigen, we generated a series of B cell lines expressing IgG1 BCRs or IgM BCRs with either high or low affinity for the hapten 4-hydroxy-3-iodo-5-nitrophenyl (NIP). J558L cells expressing an endogenous Igλ1 light chain and Igβ and a stably transfected Igα containing in its C terminus a yellow fluorescent protein (Igα-YFP) were further transfected with cDNAs encoding either high- or low-affinity versions of the NIP-specific γ1-B1-8 or μ-B1-8 heavy chains that contained cyan fluorescent proteins (CFPs) in their C termini ($\gamma1^{hi}$, $\gamma1^{lo}$, μ^{hi}, and μ^{lo}) (Figure 1A). As previously reported (Allen et al., 1988; Shih et al., 2002a; Shih et al., 2002b), we found that $\gamma1^{hi}$ and $\gamma1^{lo}$ Abs showed a 50-fold difference in affinity (K_A, 5.2×10^8 versus 9.9×10^6) for an NIP-conjugated peptide, STGKTASA *C*TSGASSTGSHis12 (NIP-H12) (Liu et al., 2010). J558L cells lines stably expressing equivalent amount of $\gamma1^{hi}$, $\gamma1^{lo}$, μ^{hi}, or μ^{lo} BCRs were acquired by cell sorting (Figure 1A and Figures S1A–S1C). By fluorescence microscopy, we confirmed that each cell line expressed Igα-YFP and a mIg-CFP on their surfaces and that the BCRs recognized NIP (Figures S1A–S1C). Using TIRF microscopy (TIRFM), we previously compared the responses of μ^{lo} and μ^{hi} cells encountering NIP-HIS12-containing fluid lipid bilayers and reported that BCR oligomerization, growth of BCR microclusters, recruitment of Syk kinase to the microclusters, and calcium fluxes were affinity-dependent events (Liu et al., 2010). Here, we compare the early stages of B cell activation for cells expressing BCRs with the same affinity for the NIP-H12 but of the IgM versus IgG1 isotype.

Cells were labeled with Alexa 568-conjugated Fab IgG- or IgM-specific antibodies (Alexa 568-Fab anti-IgG or anti-IgM) under conditions that allowed tracking of individual BCRs placed on lipid bilayers containing monovalent peptide antigen NIP-H12 and monitored by TIRFM as previously reported (Tolar et al., 2009a) (Movie S1). We analyzed these single BCR TIRF images recorded in a 10 s time course to determine the instant diffusion coefficients, D_0, and the trajectory footprints for individual BCRs as described (Tolar et al., 2009a). In the absence of antigen, IgM BCRs showed a significantly lower MSD compared to IgG1 BCRs (Figure 1B). The cumulative probability distribution (CPD) plots also indicated that in the absence of antigen, a fraction of the IgM BCRs are less mobile compared to IgG1 BCRs (Figure 1C). Considering a diffusion cutoff of 0.01 $\mu m^2/s$ immobile as previously described (Tolar et al., 2009a), we found that a comparable fraction of both $\gamma1^{hi}$ and μ^{hi} BCRs are immobile in the absence of antigen (Figure 1C), consistent with an earlier study (Tolar et al., 2009a). However, within the more mobile population of BCRs with D_0 value greater than 0.1 $\mu m^2/s$, IgM BCRs are less mobile than IgG1 BCRs (Figure 1C). The D_0 scatter plots also show μ-High BCRs are less mobile than $\gamma1^{hi}$ BCRs in the absence of antigen (approximately, 0.1 $\mu m^2/s$ versus 0.14 $\mu m^2/s$) (Figure 1D). Similar results were acquired when comparing $\gamma1^{lo}$ and μ^{lo} BCRs (Figures S1D–S1F and Movie S2). It will be of interest to determine the relevance of these observations to possible antigen-independent functions of BCRs, for example, "tonic" signaling.

The behavior of IgM versus IgG1 BCRs was strikingly different when cells were placed on antigen-containing bilayers. The γ1-High BCRs showed a significantly smaller area of confinement as compared to μ-High BCRs (0.07 μm^2 versus 0.11 μm^2) (Figure 1B), a larger fraction of immobilized oligomers (62% versus 54%) (Figure 1C) and a lower mean D_0 (0.035 versus 0.039 $\mu m^2/s$) (Figure 1D). Similar results were acquired when $\gamma1^{lo}$ BCRs were compared to μ^{lo} BCRs (Figures S1D–S1F and Movie S2).

The behavior of IgM and IgG1 BCRs was also examined in splenic B cells obtained from Igα-YFP transgenic C57BL/6 mice. To obtain a sufficient number of IgG expressing B cells for analysis, purified B cells were cultured for 72 hr with 40 μg/ml LPS and 20ng/ml recombinant mouse IL-4 (Figure S2A, B), a well-established protocol for inducing IgG1 class switching (Kaisho et al., 1997). B cells were labeled with Alexa568-Fab anti-IgM or anti-IgG Fc portion under conditions that allowed tracking of individual BCRs. When placed on lipid bilayers without antigen both IgG1 BCRs and IgM BCRs were mobile with just 12% of the BCRs in immobile fractions but IgM BCRs were less mobile as compared to IgG1 BCRs (Figure 2E-G). When placed on lipid bilayers containing F(ab′)2 anti-mouse Ig light chain [F(ab′)2 anti-L] as a surrogate antigen to crosslink the BCRs, IgG1 BCRs showed a significantly smaller area of confinement as compared to IgM BCRs (0.18 μm^2 versus 0.22 μm^2) (Figure 1E), a larger fraction of immobilized oligomers (54% versus 44%) (Figure 1F) and a lower mean D_0 (0.045 versus 0.051 $\mu m^2/s$) (Figure 1G), consistent with the results from J558L cells.

IgG1 BCR Microclusters Grow More Rapidly to Larger Sizes Than IgM BCR Microclusters

Following oligomerization, BCR microclusters grow with time in both the number of BCRs within a cluster (FI) and the size (diameter) of the cluster. We recently provided evidence that

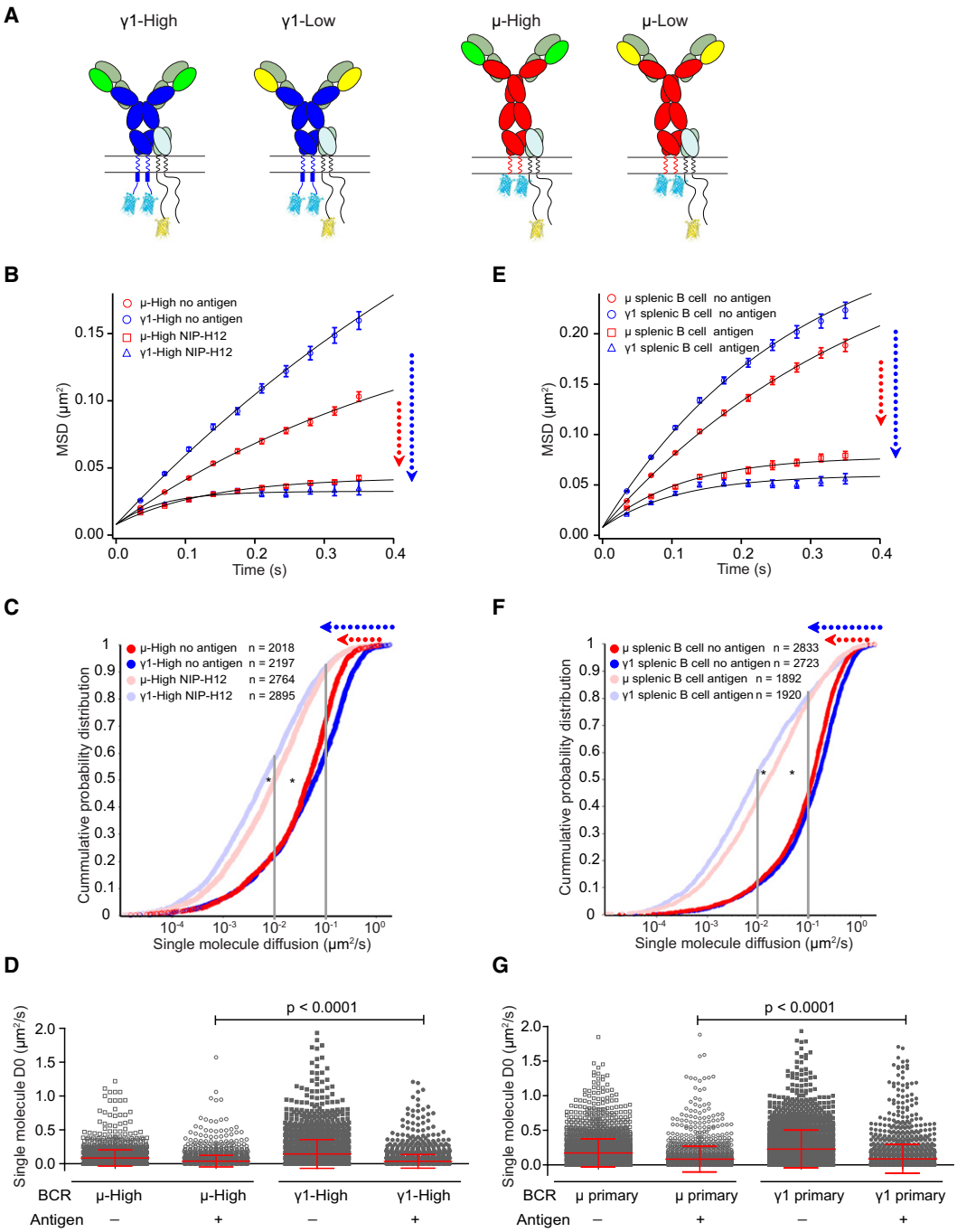

Figure 1. Quantification of the Behaviors of IgG1 and IgM BCRs upon Antigen Binding

(A) Shown are schematic representations of $\gamma 1^{hi}$, $\gamma 1^{lo}$, μ^{hi}, and μ^{lo} BCRs expressed by J558L cells used in this study. Depicted are Igλ1 light chain (light green), Igβ (light blue), and a stably transfected Igα (light blue) containing YFP (yellow). Also depicted are Cγ1-3 (dark blue), Cμ1-4 (red), high-affinity V_H (dark green), and low-affinity V_H (bright yellow).

(B–G) The D_0 values for all BCR molecules from $\gamma 1^{hi}$ and μ^{hi} J558L cells (B–D) or γ1- and μ-BCR-expressing splenic B cells (E-G) that were placed on planar lipid bilayers lacking antigen or containing antigen. The results were displayed as mean square displacement (MSD) plots (B and E), cumulative probability distribution (CPD) plots (C and F), or mean ± SD scattered plot (D and G). In MSD and CPD plots, the arrows indicate the change in the MSD (B and E) or single molecule diffusion (C and F) for IgM (red) and IgG1 BCRs (blue). Data represent single BCR molecules of indicated numbers (C and F) for each condition from three independent experiments. The MSD plots in (B) and (E) were further mathematically fitted into a confined diffusion model by an exponential function to acquire the size of the confinement microdomains as detailed in methods section. Significant difference in Kolmogorov-Smirnov test is indicated (*$p < 0.0001$) in (C) and (F). One-tailed t tests were performed for statistical comparisons in (D) and (G). The results given for μ^{hi} J558L cells were recently reported (Liu et al., 2010).

See also Figure S1.

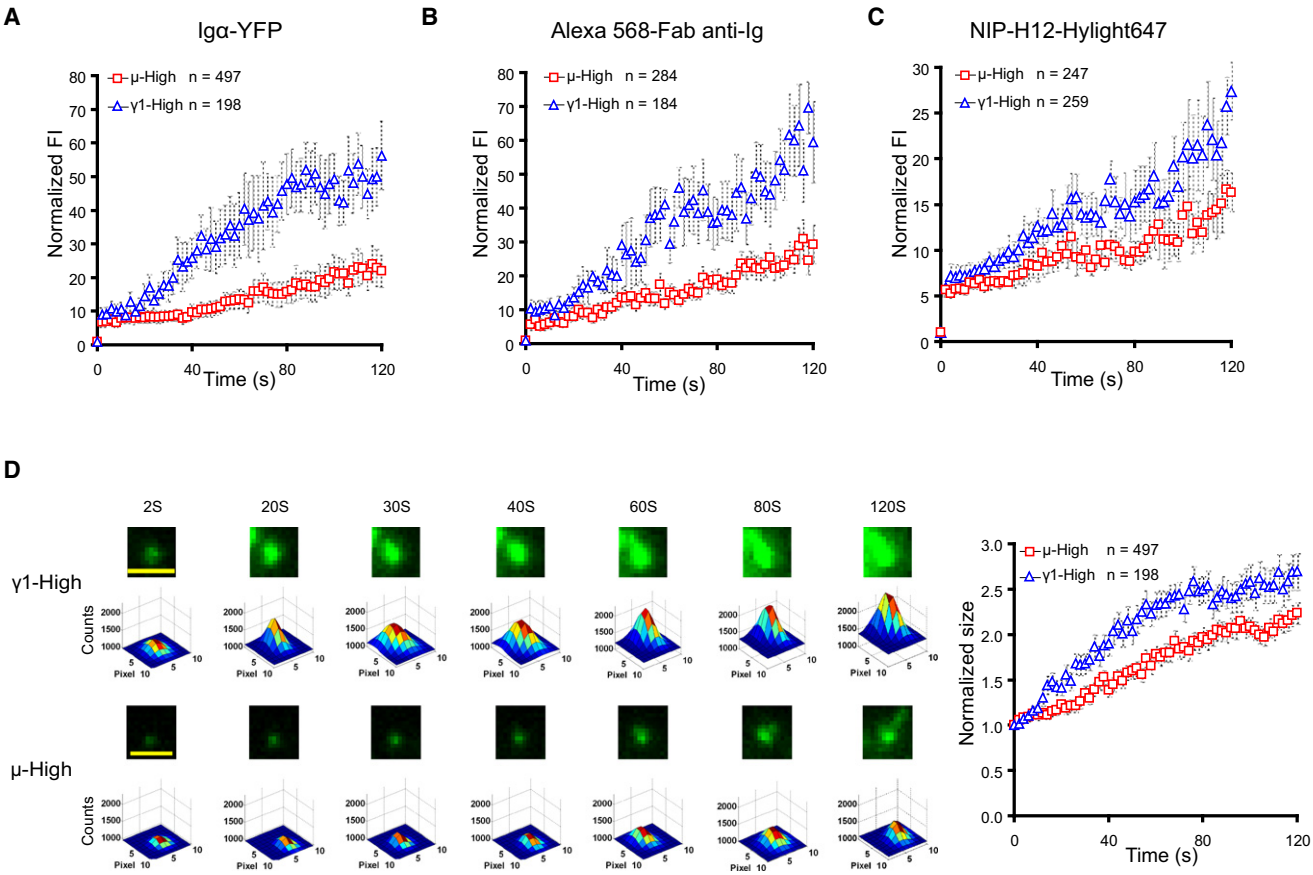

Figure 2. IgG1 BCR Microclusters Show Enhanced Ability to Grow Compared to IgM BCR Microclusters

(A–C) The growth in FI of BCR microclusters were examined by simultaneously imaging Igα-YFP with either Alexa 568-Fab-anti-IgG or -anti-IgM or NIP-H12-Hylight647 in multiple paneled two-color TIRFM.

(D) TIRF images and pseudo color 2D Gaussian images of one typical BCR microcluster examined by Igα-YFP are shown at the indicated times from $\gamma1^{hi}$ versus μ^{hi} J558L cells. Individual BCR microclusters at each time point were fitted by a 2D Gaussian function for precise 2D (x and y) coordinates, integral FI profiles, and FWHM as detailed in Experimental Procedures. For the fitted 2D Gaussian images, the display range is all set from 1000 to 2000, and for the original 16 bit Igα-YFP TIRF images from 944 to 1568, to allow direct visional comparisons. Scale bar is 1.5 μm. The data represent the mean ± SEM of the indicated number of BCR microclusters examined by Igα-YFP (A), Alexa 568 Fab-anti-Ig (B), or antigen microclusters examined by NIP-H12-Hylight647 (C) in three independent experiments. (D) Shown in the right panel is the mean ± SEM of the size of the indicated number of Igα-YFP BCR microclusters in three independent experiments. The statistical test used to compare the data is described in Experimental Procedures. The results given for μ^{hi} J558L cells were recently reported (Liu et al., 2010). See also Figure S2.

the growth of BCR microclusters is antigen affinity dependent for IgM BCRs (Liu et al., 2010). To determine if the growth of IgG1 BCR and IgM BCR microclusters are similar independently of affinity, $\gamma1^{hi}$, μ^{hi}, $\gamma1^{lo}$, and μ^{lo} J558L cells were labeled with Alexa 568-Fab anti-IgM or -IgG and placed on lipid bilayers containing NIP-H12-Hylight647 and imaged in multiple paneled two-color TIRFM (Movies S3–S5). Each BCR microcluster at each time point was fitted mathematically to a 2D Gaussian function (Holtzer et al., 2007) to acquire accurate information on the size and FI of each microcluster for quantitative comparisons. For each microcluster, the 2D Gaussian fit yields the parameters of position (x_c, y_c) for x and y coordinates, integrated FI (I) for the quantification of FI, and full width at half maximum peak height (σ_x, σ_y) of the intensity distribution in x and y directions to quantify the size (diameter) of the cluster (Holtzer et al., 2007). Only the first 120 s of each track of the microclusters was analyzed to minimize tracking and Gaussian fitting errors that arise from microclusters merging or overlapping with time.

Comparing the increase in FI of μ^{hi} and $\gamma1^{hi}$ BCR microclusters quantified from either Igα-YFP (Figure 2A and Movie S3) or Alexa 568-anti-Ig images (Figure 2B and Movie S3), we observed that the IgG1 BCRs grew more rapidly, increasing in FI almost 50-fold over the 120 s time course, in contrast to IgM BCR microclusters that increased only 20-fold. When the FI of the antigen in the bilayer, NIP-H12-Hylight647, was quantified, we also observed that the IgG1 BCRs grew more rapidly reaching higher FI as compared to IgM BCRs (Figure 2C, Figure S2C, and Movie S4). For IgM BCRs, the growth of the microclusters was similar measuring the FI of either the BCRs or the antigen. However, the increase in antigen FI for the IgG1 BCR microclusters was not as large as that observed when quantifying the FI of IgG1 BCR clusters from either Igα-YFP or Alexa 568- anti-Ig images

(Figures 2A–2C). Thus, for IgG1 BCRs, the microclusters grew more rapidly in their IgG1 BCR content as compared to their antigen content. Similar results were acquired when comparing $\gamma1^{lo}$ and μ^{lo} BCRs (Figure S2D and Movie S5). These observations raise the interesting possibility that a portion of IgG1 BCRs are recruited to the growing microclusters in an antigen-independent fashion. We also determined that independently of affinity, the IgG1 BCR microclusters grew in diameter faster, forming larger microclusters as compared to IgM BCR microclusters (Figure 2D and Figures S2D and S2E).

IgG1 BCRs Are Enhanced in Their Ability to Accumulate Antigen in the Contact Area

When B cells are placed on antigen-containing bilayers, the BCRs that are initially uniformly distributed over the entire B cell surface accumulate nearly completely at the interface of the B cell and the bilayer within 10 min (Figure 3A and Movie S6). Using TIRFM to image the contact area of the cells with the antigen-containing lipid bilayer in real time (Figure 3B, Figure S3A, and Movies S3–S5), we found that compared to B cells expressing IgM BCRs, B cells expressing IgG1 BCRs showed an enhanced ability to accumulate BCRs and antigen at the interface over a 120 s time course, as indicated by the increased mean FI of either Igα-YFP (Figure 3C and Figure S3B), Alexa 568-Fab-anti-Ig (Figure 3D and Figure S3C), and NIP-H12-Hylight647 (Figure 3E and Figure S3D). The accumulation of the BCRs was antigen dependent in that no accumulation of BCRs occurred when the cells were placed on bilayers that did not contain antigen (Figure 3A and Movie S6). Additionally, we found that IgG1 BCRs accumulated more rapidly in the interface than did antigen.

Similar results were obtained in an analysis of IgM and IgG1 BCR expressing splenic B cells from Igα-YFP Tg mice. IgG1-expressing B cells were obtained by incubating purified splenic B cells with LPS and IL-4 as described above (Figures S2A and S2B). The surface expression of IgM and IgG1 BCRs was quantified by analyzing the equatorial mean Igα-YFP FI of the cells imaged in an epifluorescence illumination mode (Figure 4A). Only the TIRF images of B cells expressing similar amounts of IgM and IgG1 BCRs were included in the analysis (Figure 4B). Cells were labeled with Alexa 568-Fab anti-IgM or anti-IgG Fc portion (Figure 4A) and placed on lipid bilayers containing F(ab′)2 anti-L to crosslink BCRs. After 10 min, we observed that IgG1-B cells accumulated significantly more Igα-YFP and Alexa 647-F(ab′)2 anti-L into the contact area as compared to IgM-B cells (Figures 4C and 4D). Following the kinetics of the accumulation of IgM and IgG1 BCRs in splenic B cells, we observed that BCR microclusters formed at the initial contact points of the primary B cells with F(ab′)2 anti-L containing lipid bilayers, and beginning at 24 s, the BCR microclusters merged and overlapped because the splenic B cells spread over the F(ab′)2 anti-L-containing lipid bilayers (Figures S4A and S4B and Movie S7). As compared to IgM-B cells, IgG1-B cells accumulated BCRs in the contact area more rapidly and in larger amounts as measured by Igα-YFP (Figure S4C) or Alexa 568-Fab anti-Ig (Figure S4D). Additionally, we observed that the IgG1 BCRs accumulated into the contact area in larger amounts than did the surrogate antigen, Alexa 647-F(ab′)2 anti-L (Figures S4C–S4E).

IgG1 BCRs Rapidly Undergo BCR Oligomerization-Induced Cytoplasmic Changes and Initiate Signaling

We previously showed by FRET analyses that following antigen binding, both the BCRs' ectodomains and cytoplasmic domains cluster into close molecular proximity and exhibit FRET. From this "closed" configuration, the cytoplasmic domains subsequently lose FRET, coming into an "open" form that occurs simultaneously with the phosphorylation of the BCR's ITAMs and recruitment of Syk (Sohn et al., 2008; Tolar et al., 2005). We analyzed FRET in J558L cells expressing the FRET acceptor, Igα-YFP, and the FRET donor, either γ1-CFP or μ-CFP mIg, with time after the cells were placed on NIP-H12-containing fluid lipid bilayers. Prior to antigen activation, at time 0, both IgM- and IgG1-expressing cells showed a significant amount of intramolecular FRET as previously described (Tolar et al., 2005) because of the close molecular proximity of the CFP-containing cytoplasmic domains of the mIg and YFP-containing Igα in the BCR (Figure 5A; Figure S5A). However, with NIP-H12 engagement, FRET increased rapidly, reflecting the acquisition of intermolecular FRET between the cytoplasmic domains of BCRs as they clustered into close molecular proximity (Figure 5A and Figure S5A). We found that although IgG1 BCRs and IgM BCRs appeared to acquire FRET at the same rate, IgG1 BCRs, independently of affinity, reached higher FRET efficiency as compared to IgM BCRs, indicating a greater degree of clustering (Figure 5B and Figure S5B). We also analyzed the subsequent loss of FRET in the IgM and IgG1 BCR clusters. The averaged FRET decay plots were fitted into an exponential decay function to calculate the half life of FRET loss, τ50 (Figure 5C and Figure S5C). We determined that independently of affinity, the τ50 for IgG1 BCRs was significantly faster as compared to IgM BCRs (Figure 5C and Figure S5C). We interpret these results to mean that compared to IgM BCRs, the cytoplasmic domains of IgG1 BCRs in microclusters more rapidly come into an "open" active conformation. Consistent with this observation, we determined by TIRFM that independent of affinity, cells expressing IgG1 BCRs accumulated significantly more pSyk and BCRs into the contact area compared to IgM BCRs (Figures 5D and 5E and Figures S5D and S5E). A similar observation was made for IgM- and IgG1-expressing splenic B cells (Figure 4E). We also observed that switched IgG1 splenic B cells showed enhanced calcium responses as compared to IgM B cells (data not shown) similar to that previously reported (Engels et al., 2009; Horikawa et al., 2007; Waisman et al., 2007; Wakabayashi et al., 2002).

The Cytoplasmic Tail of mIgG1 Mediates Enhanced BCR Microcluster Growth and Antigen Accumulation

To determine what feature of the IgG1 BCRs contributed to the enhancement of BCR clustering, we generated cell lines that expressed the BCR chimeras shown in Figure 6A. Cells were labeled with Alexa 568-Fab-anti-Ig and placed on NIP-H12-Hylight647-containing bilayers, and the growth of both BCR and antigen clusters was quantified by imaging Igα-YFP and NIP-H12-Hylight647 in multiple paneled two-color TIRFM. As compared to γ1-WT BCRs, the γ1-Cyto μ BCRs were impaired in their ability to grow and were similar in their growth to μ-WT BCRs (Figures 6B and 6C). Conversely, μ-Cyto γ1 BCRs behaved equivalently to γ1-WT BCRs (Figures 6B and

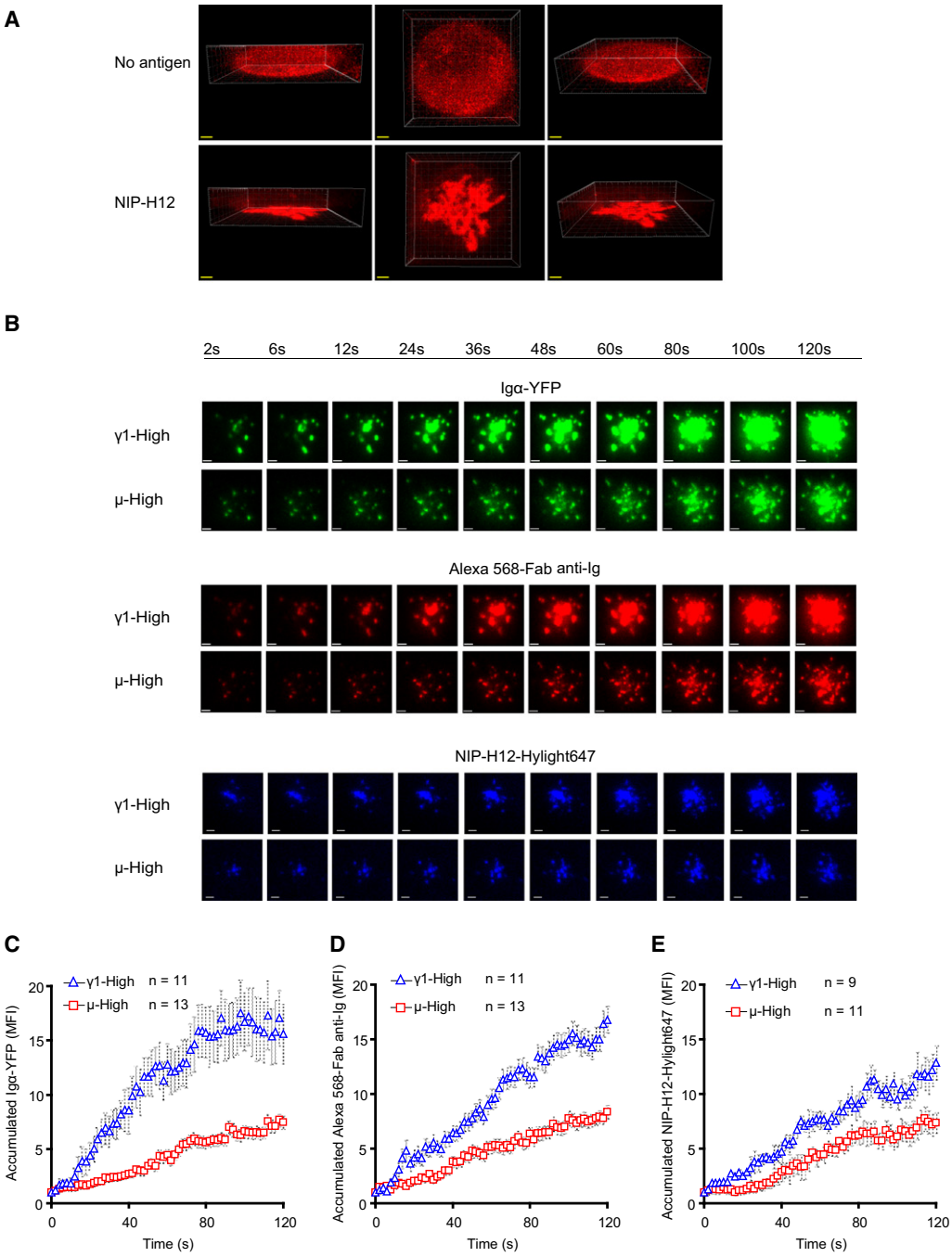

Figure 3. IgG1 BCRs Are Enhanced in Their Ability to Accumulate Antigen in the Contact Area with Antigen-Containing Lipid Bilayers

(A) Shown are 3D images of $\gamma1^{hi}$ J558L cells stained with Alexa 568-Fab-anti-IgG placed on planar lipid bilayers containing no antigen (top panels) or NIP-H12 (lower panels). The 3D images are shown from three different views: side (left panel), top (middle panel) and 45° angle (right panel) (also see Movie S6). Scale bar is 1.0 μm.

(B–D) Multiple paneled two-color TIRF images are shown at the indicated time points over a course of 120 s from $\gamma1^{hi}$ and μ^{hi} J558L cells placed on NIP-H12-containing planar lipid bilayers. The BCR microclusters were examined by simultaneously imaging Igα-YFP (green) and Alexa 568-Fab-anti-IgM or anti-IgG (red), and antigen microclusters were examined by imaging NIP-H12-Hylight647 (blue). For the original 16 bit TIRF images, the display range was set from 944 to 1968 (Igα-YFP), from 944 to 1600 (Alexa 568-Fab-anti-Ig), and from 944 to 1280 (NIP-H12-Hylight647) in both $\gamma1^{hi}$ and μ^{hi} cells to allow direct visional comparisons. Scale bar is 1.5 μm. The normalized mean FIs within the contact area of Igα-YFP (C), Alexa 568-Fab-anti-IgM or anti-IgG (D), or NIP-H12-Hylight647 (E) are given over 120 s for either μ^{hi} or $\gamma1^{hi}$ J558L cells placed on antigen-containing planar lipid bilayers. The data represent the mean ± SEM of indicated numbers of cells in three independent experiments. The statistical test used to compare the data is described in Experimental Procedures. The results given for μ^{hi} cells were recently reported (Liu et al., 2010).

See also Figure S3.

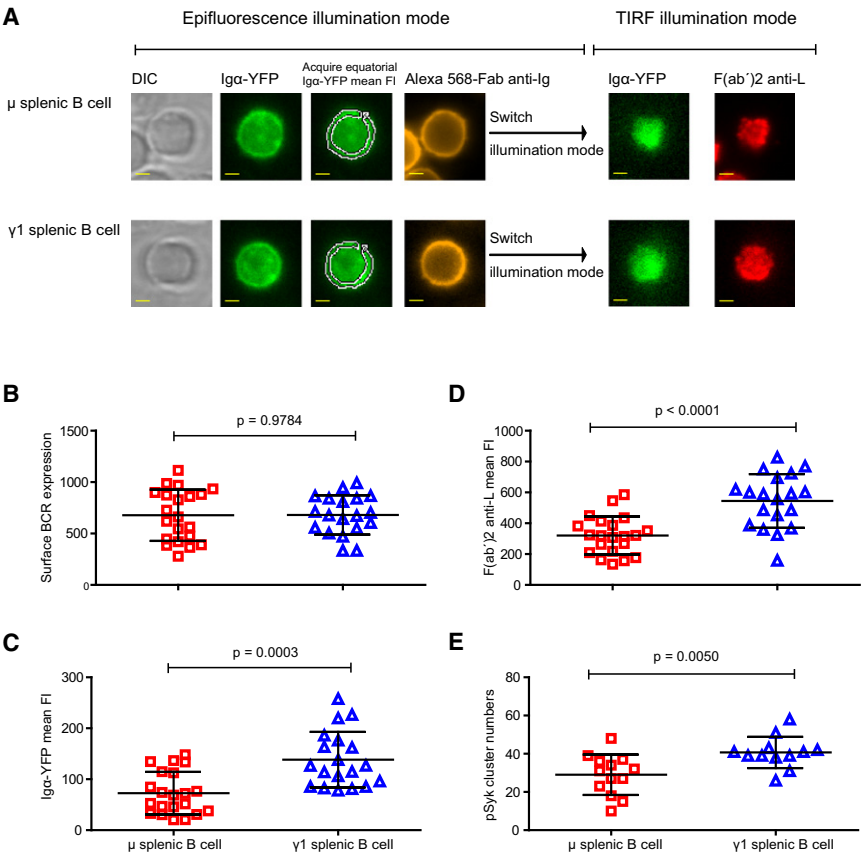

Figure 4. IgG1-Expressing Splenic B Cells Show Significantly Enhanced Ability to Accumulate Antigen and pSyk into the Contact Interface with Antigen-Containing Lipid Bilayers

(A–E) Splenic B cells from Igα-YFP Tg C57BL/6 mice were incubated with LPS and IL-4 for 72 hr to induce class switching. B cells were labeled with Alexa 568-Fab anti-IgM or anti-IgG Fc portion, placed on lipid bilayers containing biotinylated ICAM-1 and Alexa 647-F(ab′)2 anti-L for 10 min, fixed, and imaged by TIRFM. For detection of pSyk recruitment to the contact area, splenic B cells were fixed, permeabilized, and stained with antibodies specific for pSyk as detailed in Experimental Procedures. (A) Given are two-color images for Igα-YFP (green) and Alexa568-Fab anti-IgM (or anti-IgG) (yellow) of B cells illuminated in either an epifluorescence mode (left) or a TIRF mode (right). The area of the Igα-YFP epifluorescence image from which the mean FI of equatorial Igα-YFP FI profile was acquired is outlined in white. Scale bar is 1.5 μm. Given are the statistical comparison for the amount of surface BCR as quantified from equatorial Igα-YFP mean FI profile (B), the accumulated Igα-YFP (C) and Alexa 647-F(ab′)2 anti-L (D) into the contact area, and the number of pSyk clusters in the contact area (E). Each dot represents one cell analyzed in three independent experiments, and bars represent the mean ± SD. Two-tailed t tests were performed for the statistical comparisons.
See also Figure S4.

6C). Within the γ1 cytoplasmic tail, the only residue that has been shown to be involved in signaling is the tyrosine present in the membrane proximal 20 residues of the tail (Engels et al., 2009). Surprisingly, the μ-Cyto N12 γ1 and γ-Cyto N12 γ1 BCRs that contained only the 12 membrane proximal residues of the mIgG tail lacking this tyrosine, behaved like the γ-WT BCRs (Figures 6B and 6C), suggesting that the tyrosine was not involved in the enhanced clustering. We confirmed that J558 cells expressing γ1 chains with the C-terminal Y→F mutation (γ1-Y384F) (Figure 6A) behaved like γ1-WT (Figures 6B and 6C). We also observed no effect of swapping the TM domains of the μ chain with that of the γ1 chain in μ-TMγ1-Cyto μ BCRs (Figures 6B and 6C). When comparing the accumulation of the antigen, NIP-H12-Hylight647, as compared to the BCRs themselves (Figure S6), it was apparent that the antigen-independent accumulation of IgG1 BCRs is a function of the γ tail. When quantifying the ability of the cell lines expressing the various BCR constructs to accumulate BCRs and antigens in the interface of the cells and the antigen-containing lipid bilayers, we observed that μ-Cyto γ1, μ-Cyto N12 γ1, γ1-Cyto N12 γ1, and γ1-Y384F BCRs all behaved equivalently to γ1-WT BCRs (Figures 6D and 6E).

We also determined the functions of the various mIgG1 constructs when expressed in splenic B cells. Purified splenic B cells from C57BL/6 mice were transfected with constructs encoding γ1-WT, γ1-Y384F, γ1-Cyto N12 γ1, or γ1-Cyto μ heavy chains fused, in each case, with a C terminus CFP tag. The transfected B cells were labeled with Alexa 568-Fab anti-IgG Fc, and placed on lipid bilayers containing Alexa 647-conjugated F(ab′)2 anti-IgG F(ab′)2 to crosslink the BCRs. After 10 min, the B cells were fixed, permeabilized and stained with rabbit antibodies specific for pSyk, detected using Alexa 488-conjugated F(ab′)2 anti-rabbit IgG. Four-colored TIRF images were acquired for each individual IgG-positive splenic B cell (Figure 7A). Also taken was an Alexa 568-Fab anti-IgG Fc image at epifluorescence illumination mode (Figure 7A) and only B cells expressing comparable amounts of surface IgG1 BCRs (Figure 7B) were included in the analysis. Primary B cells expressing γ1-WT, γ1-Y384F, or γ1-Cyto N12 γ1 BCRs accumulated significantly more BCRs, antigen, and pSyk into the contact area compared to γ1-Cyto μ BCRs (Figure 7B). We also imaged and compared the calcium responses of these transfected splenic B cells upon encountering of membrane-bound antigens (Figure S7A) and found that the splenic B cells expressing γ1-WT BCRs showed elevated calcium responses as compared to cells expressing γ1-Cyto μ (Figure 7C and Figures S7B and S7C). The splenic B cells expressing either γ1-Y384F or γ1-Cyto N12 γ1 also showed significantly enhanced calcium response as compared to γ1-Cyto μ BCRs, comparable to γ1-WT BCRs (Figure 7C and Figures S7B and S7C). The enhanced response of B cells expressing γ1-Y384F observed here for B cells encountering membrane bound antigen tethered on planar membranes is different from the observations of Engels et al. (2009), showing that this C-terminal tyrosine residue was necessary for enhanced calcium response when IgG BCRs were crosslinked by soluble antigens. As discussed below, such differences may reflect the different mode of antigen stimulation.

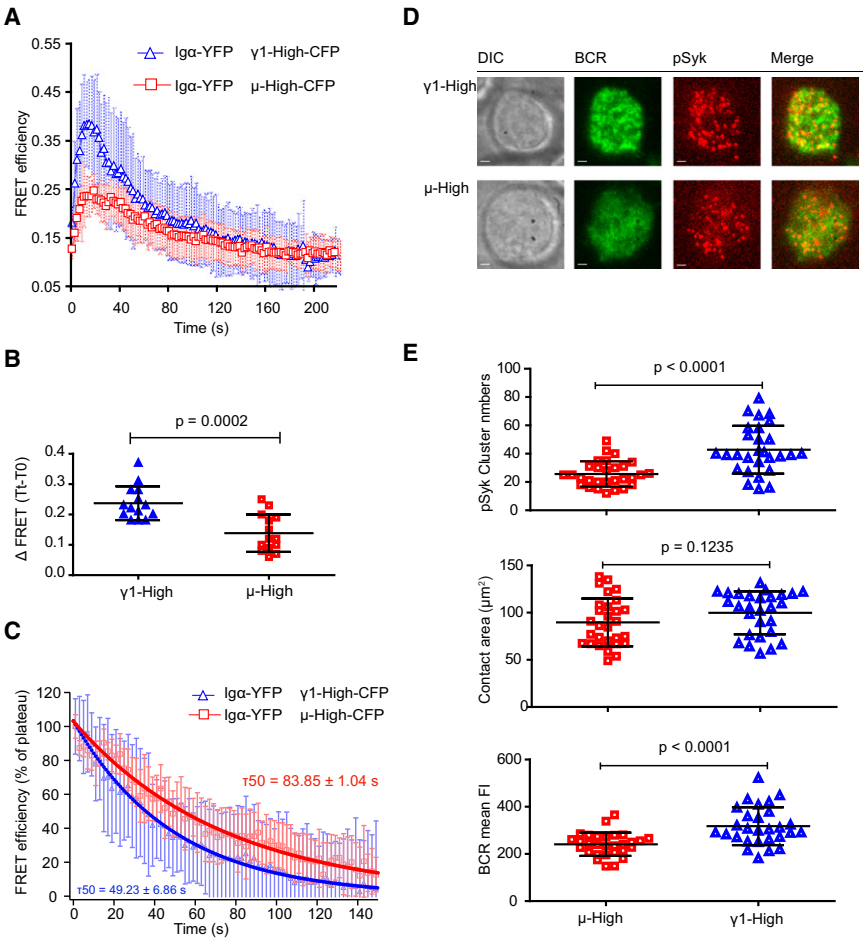

Figure 5. IgG1 BCRs Rapidly Undergo BCR Oligomerization-Induced Changes in the BCR's Cytoplasmic Domains and Recruit pSyk

(A–C) FRET efficiencies between FRET donor Igα-YFP and FRET acceptor IgH-CFP are given at the indicated times for J558L cells placed on lipid bilayers containing NIP-H12. Acquisition and analyses of CFP- and YFP-paired TIRF FRET images were as reported (Tolar et al., 2005) and detailed in Experimental Procedures. (A) Mean ± SD of FRET efficiencies are given over 240 s for $\gamma1^{hi}$ and μ^{hi}. (B) Statistical comparisons for the maximal changes in FRET (ΔFRET) from 0 and 200 s are given. The decay plots of FRET efficiencies from maximal FRET values, set at 100%, are given. (C) The decay plots were mathematically fitted into a monoexponential decay function to calculate the half life of FRET loss, τ_{50}, as detailed in Experimental Procedures.

(D and E) The $\gamma1^{hi}$ and μ^{hi} J558L cells were placed on lipid bilayers containing NIP-H12 for 10 min, fixed, permeabilized, and stained with antibodies specific for pSyk as detailed in Experimental Procedures. (D) Given are two-color TIRF images for Igα-YFP (green) and pSyk (red). For the original 16-bit TIRF images, the display range was set from 928 to 1344 (Igα-YFP) and from 928 to 992 (pSyk) in both $\gamma1^{hi}$ and μ^{hi} cells to allow direct visional comparison. Scale bar is 1.5 μm. (E) Given are the number of pSyk clusters in the contact area, the size of the contact area, and mean BCR FI of the contact area for $\gamma1^{hi}$ and μ^{hi} cells. Each dot represents one cell analyzed in three independent experiments, and bars represent the mean ± SD. Two-tailed t tests were performed for the statistical comparisons. The results given for μ^{hi} J558L cells were recently reported (Liu et al., 2010).

See also Figure S5.

DISCUSSION

A hallmark of humoral immunological memory is the rapid production of high titered, high-affinity, isotype-switched antibodies in response to antigenic challenge. Over the last several years, the molecular mechanisms by which B cells undergo isotype switching and somatic hypermutation leading to high-affinity antibodies have been described in considerable detail (McHeyzer-Williams and McHeyzer-Williams, 2005). In addition, the general rules by which antigen selection occurs at the clonal level within germinal centers during immune responses have been laid out (Dal Porto et al., 2002; Paus et al., 2006; Phan et al., 2006; Shih et al., 2002a, 2002b; Takahashi et al., 1998). However, what remains relatively poorly understood are the mechanisms acting at the cellular level by which the expression of isotype switched high-affinity BCRs provide advantages to MBCs in their ability to be reactivated by antigen.

Here, we asked if IgM BCRs and IgG1 BCRs are intrinsically similar in their ability to oligomerize and cluster, events that are prerequisite to the initiation of signaling. The ability to ask this question comes from new knowledge of the early events in the initiation of BCR signaling gained by applying high-resolution live-cell imaging techniques to describe the events that occur within seconds of antigen binding to the BCR (Batista and Harwood, 2009; Harwood and Batista, 2008; Tolar et al., 2009a, 2009b). We previously provided evidence that the events leading up to the initiation of signaling were ordered beginning with antigen engagement leading to oligomerization, BCR clustering, growth of the clusters, and changes in the cytoplasmic domains that occur simultaneously with the phosphorylation of the BCR Igα and Igβ ITAMs, all within the first minute of antigen engagement (Sohn et al., 2006, 2008; Tolar et al., 2005, 2009a, 2009b). We recently reported that these ordered early molecular events in the initiation of BCR signaling are highly sensitive to antigen affinity, thus putting the B cell affinity discrimination at the beginning of the complex B cell activation cascade (Liu et al., 2010). Concerning the behavior of BCRs of different isotypes, Batista and colleagues recently reported differences in the steady-state behaviors of IgM, IgG, and IgD BCRs in the absence of antigen that were controlled by boundaries imposed by the membrane cytoskeleton (Treanor et al., 2010). Here, we provide evidence that independently of affinity, IgG1 BCRs are enhanced in driving the early antigen-dependent events as compared to IgM BCRs and that the cytoplasmic tail of mIgG1 is both necessary and sufficient for this enhancement.

Of significant interest was the observation that the region of the mIgG1 cytoplasmic tail that conferred enhanced oligomerization and clustering was the membrane proximal 12 residues,

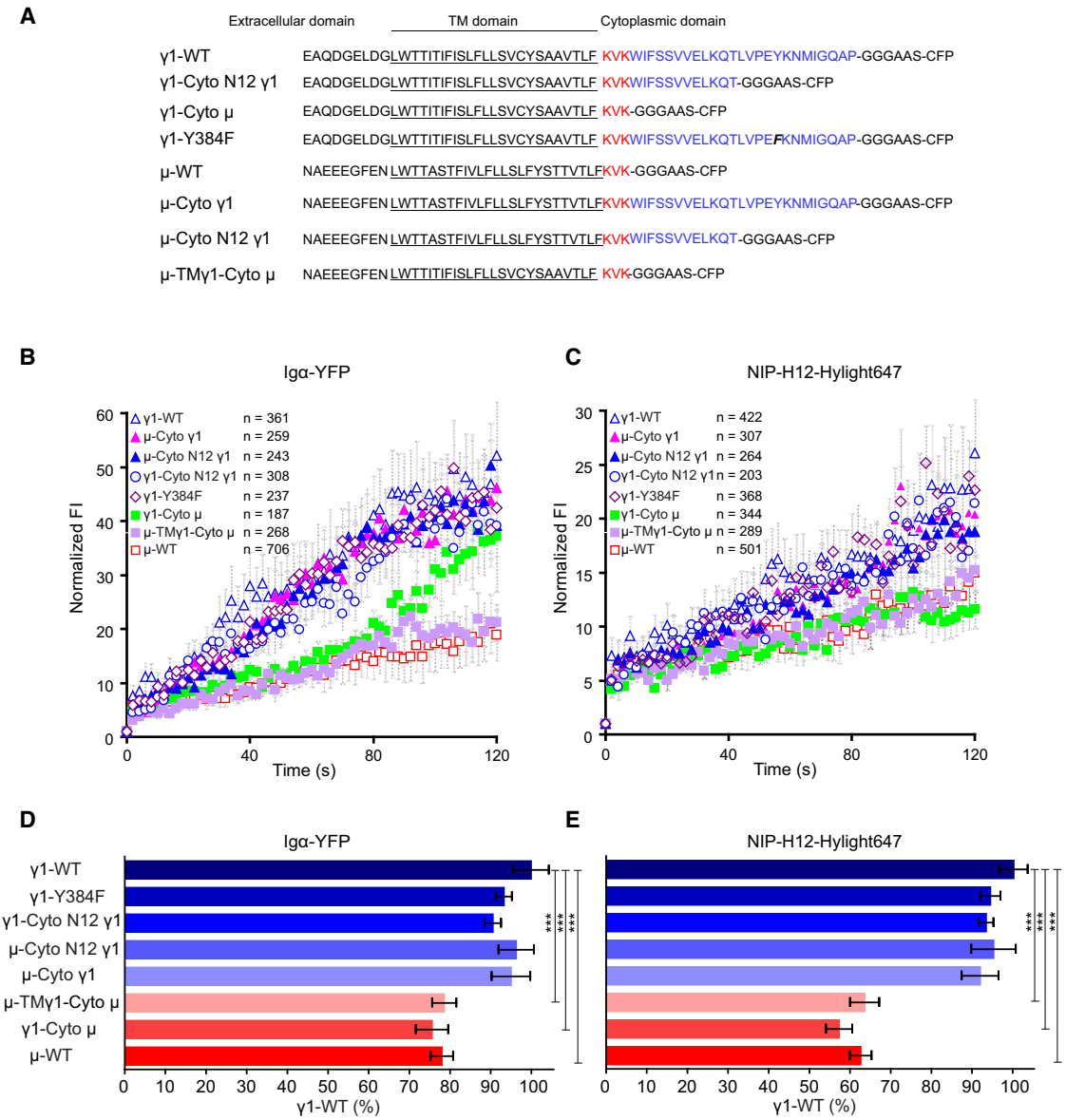

Figure 6. The Cytoplasmic Tail of IgG1 BCRs Mediates the Enhanced Growth of BCR Microclusters and the Enhanced Acquisition of BCRs and Antigen into the Contact Area of the B Cells with Antigen-Containing Lipid Bilayers

(A) The cytoplasmic amino acid sequences of γ1-WT, γ1-Cyto N12 γ1, γ1-Cyto μ, γ1-Y384F, μ-WT, μ-Cyto γ1, μ-Cyto N12 γ1, and μ-TMγ1-Cyto μ are given. J558L cells were placed on antigen-containing fluid lipid bilayers and the growth of BCR microclusters imaged by Igα-YFP (B) or antigen microclusters by NIP-H12-Hylight647 (C) over time. The data represent the mean ± SEM of the indicated numbers of BCR microclusters in at least three independent experiments. The statistical test used to compare the data is described in Experimental Procedures. (D and E) J558L cells were placed on antigen-containing lipid bilayers for 10 min, fixed, and imaged by multiple paneled two-color TIRFM for Igα-YFP (BCR) and NIP-H12-Hylight647 (antigen). Shown are the ability of the various cell lines to accumulate BCR and antigen into the contact interface as a percent of the γ1-WT. The data represents the mean ± SEM of 24–35 cells in three independent experiments. Two-tailed t tests were performed for the statistical comparisons.
See also Figure S6.

not previously recognized to play a role in BCR signaling. This region of the cytoplasmic tail does not contain the tyrosine recently shown to be necessary to drive IgG signaling to MAP kinases (Engels et al., 2009). In our experiments in which B cells were activated by membrane-bound antigens tethered to planar lipid bilayers, we found that these membrane proximal 12 residues of the cytoplasmic tail alone significantly enhanced calcium responses. This enhancement was also observed in B cells expressing the γ1-Y384F mutant mIgG1. These results differ from those of Engels et al. (2009) showing that this tyrosine was necessary for enhanced signaling when crosslinking the IgG BCRs using soluble antigens. The mechanism underlying this difference is still under investigation, but we speculate that the B cells may have different requirements for activation when

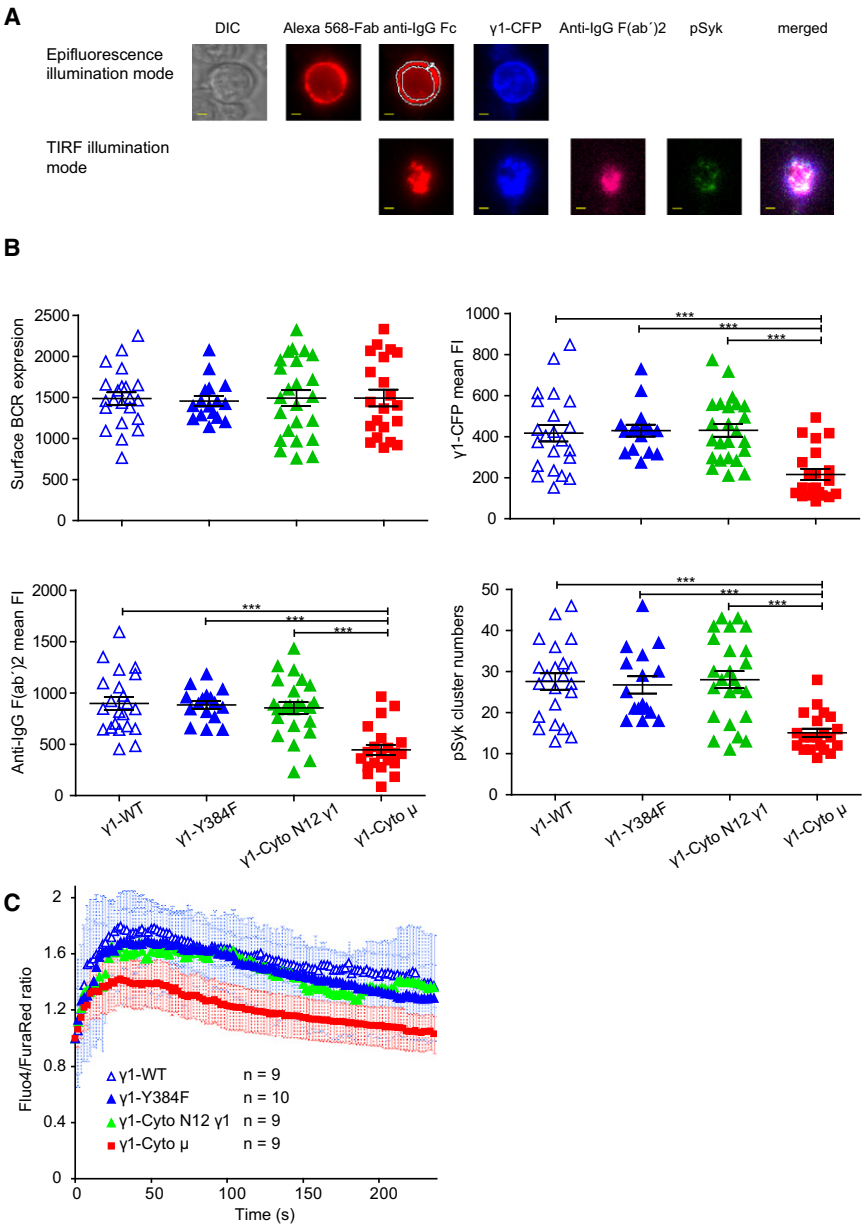

Figure 7. The Membrane Proximal Region of Cytoplasmic Tail of IgG1 BCRs Mediates the Enhanced Ability of IgG1-Splenic B Cells to Accumulate BCR, Antigen, and pSyk into the Contact Area with Antigen-Containing Lipid Bilayers and the Elevated Calcium Response

(A–C) Splenic B cells were incubated with LPS and IL-4 to induce class switching, labeled with Alexa 568-Fab anti-IgG Fc portion, and placed on lipid bilayers containing biotinylated ICAM-1 and Alexa 647-F(ab′)2 anti-IgG F(ab′)2 for 10 min. The splenic B cells were then fixed, permeabilized, and stained with antibodies specific for pSyk as detailed in Methods section. (A) Given in top panel are two colored epifluorescence images for Alexa 568-Fab anti-IgG (red) and γ1-CFP (blue) of one typical primary B cell illuminated at epifluorescence mode. Given in lower panel are the four-color TIRF images for Alexa 568-Fab anti-IgG (red), γ-CFP (blue), Alexa 647-F(ab′)2 anti-IgG F(ab′)2 (red), and anti-pSyk stained by Alexa 488-F(ab′)2 antibodies (green) for the same cell when was illuminated at TIRF mode. Scale bar is 1.5 μm. (B) Given are the statistical comparisons of the amount of surface IgG1 BCR expression, the accumulated BCR (γ1-CFP), antigen [Alexa 647-F(ab′)2 anti-IgG F(ab′)2], and pSyk into the contact area. Each dot represents one cell analyzed in three independent experiments, and bars represent the mean ± SEM. Two-tailed t tests were performed for the statistical comparisons. (C) Splenic B cells expressing similar amount of γ1-WT, γ1-Y384F, γ1-Cyto N12 γ1, and γ1-Cyto μ BCRs acquired from cell sorting were placed on antigen-containing lipid bilayers, and the calcium responses were measured by time-lapse epifluorescence microscopy. Acquisition and analyses of Fluo4 to FuraRed ratio images are detailed in Experimental Procedures. Kinetics of the calcium response in 4 min is shown as mean ± SD for indicated number of cells in three independent experiments.
See also Figure S7.

responding to soluble antigens versus membrane-bound antigens. Precedence for this comes from the studies of Batista and colleagues, who found that CD19 was required for B cell activation by membrane-bound antigen, but not by soluble antigen (Depoil et al., 2008). We previously reported that the association of the BCRs with lipid rafts required Src kinase activity when cells were stimulated by soluble antigens (Sohn et al., 2006), but not when stimulated by membrane bound antigens (Sohn et al., 2008).

We recently provided evidence that the membrane proximal ectodomains of mIgG1 and mIgM appeared to oligomerize similarly (Tolar et al., 2009a). The results presented here indicate that even though the mIgG1 and mIgM ectodomains may have the same propensity to oligomerize, the mIgG1 cytoplasmic tail further promotes oligomerization and clustering. The identification of this activity of the mIgG1 tail and future studies to understand the molecular mechanism by which it promotes clustering may lead important insights into the mechanisms underlying B cell abnormalities resulting from excessive BCR signaling, including autoimmunity and BCR signaling-dependent B cell tumorigenesis. Indeed, we recently provided evidence that the IgM BCRs in activated B cell-like subtype of diffuse large B cell lymphomas, DLBCLs, that are dependent on BCRs for their survival spontaneously form prominent immobile clusters in the plasma membrane similar to antigen stimulated BCRs (Davis et al., 2010). These results suggest the possibility that alterations in critical features of the BCRs that promote oligomerization may lead to spontaneous chronic activation. Understanding the molecular basis of the ability of the IgG1 tail to enhance early events in B cell activation will be important in

informing us further about the mechanisms of BCR clustering and their regulation.

EXPERIMENTAL PROCEDURES

Mice, Cells, Antibodies, Plasmids, and Transfections

Primary B cells were isolated from spleens of Igα-YFP Tg C57BL/6 mice generated and characterized in our lab or normal C57BL/6 mice by negative selection using MACS^R sorting as described (Tolar et al., 2009a). Mice were treated in accordance with guidelines approved by the NIH Animal Care and Use Committee. To induce class switching of IgM BCRs to IgG1 BCRs, we incubated the purified spleen B cells from Igα-YFP Tg mice with 40 μg/ml LPS and 20 ng/ml recombinant mouse IL-4 for 72 hr following a well-established protocol (Kaisho et al., 1997). Purified unconjugated Fab goat anti-mouse Fc IgM (anti-IgM), F(ab′)2 goat anti-mouse IgG F(ab′)2, goat anti-mouse Ig light chain (anti-L), and goat anti-mouse IgG Fc portion were purchased from Jackson ImmunoResearch. Detailed lists of all the antibodies used in this study are provided as Supplemental Information. Plasmids expressing Igα-YFP were constructed as described (Sohn et al., 2006). Plasmids expressing γ1-B1-8 fused with a C terminus CFP through the linker peptide, GGGAAS (γ1-B1-8-CFP), were constructed as described (Tolar et al., 2005). Using the γ1-B1-8-CFP plasmid as a template, γ1-B1-8-High-CFP (γ1-High) and γ1-B1-8^{lo}-CFP (γ1^{lo}) were generated using a QuikChange II XL Site-Directed Mutagenesis Kit (Stratagene). The detailed mutagenesis procedures and acquisition of γ1^{hi} and γ1^{lo} J558L cells by transfection and cell sorting are provided in Supplemental Information.

Cytoplasmic Tail Chimeric γ1-High or μ-High Mutants

To construct the cytoplasmic tail chimera γ1-High and μ-High mutants, γ1-B1-8-High-CFP (γ1-WT) or μ-B1-8-High-CFP (μ-WT) plasmids were respectively used as parent plasmids. Based on γ1-WT, γ1-Cyto N12 γ1, γ1-Cyto μ and γ1-Y384F cytoplasmic tail mutant were acquired using primer A-C respectively (Figure S6) in QuikChange™ II XL Site-Directed Mutagenesis Kit (Stratagene). Similarly, based on μ-WT, μ-Cyto γ1, μ-Cyto N12 γ1 and μ-TMγ1-Cyto μ are acquired using primer D-G respectively (Figure S6) in mutagenesis polymerase chain reaction (PCR). All the cytoplasmic amino acid sequences and schematic presentations of these WT or mutant IgM or IgG1 heavy chain constructs are given in Figure 6A and Figure S6. We have provided detailed experimental procedures to produce these constructs in supplemental information. Transfections of γ1-WT, γ1-Y384F, γ1-Cyto N12 γ1, or γ1-Cyto μ constructs into purified splenic B cells from C57BL/6 mice were performed using an optimized Amaxa protocol for stimulated C57BL/6 mouse primary spleen B cells with an Amaxa Nucleofector Kit. Briefly, splenic B cells were purified and enriched from the spleen of 10-week-old C57BL/6 mice by negative selection using MACS^R sorting. Purified splenic B cells were incubated overnight with 50 μg/ml LPS. The LPS-stimulated B cells were transfected with these DNA constructs, respectively, using Amaxa mouse B cells Nucleofector solutions and transfection program of Z-001. Transfected B cells were cultured overnight and imaged the next day.

Two-Color Time-Lapse Live-Cell Imaging by TIRFM

Cells were placed on planar fluid lipid bilayers containing NIP hapten antigen or biotinylated anti-Ig surrogate antigen prepared as described (Tolar et al., 2009a) and provided in detail in Supplemental Information. TIRF images were acquired at 37°C on a heated stage by an Olympus IX-81 microscope supported by a TIRF port, CascadeII 512 × 512 electron-multiplying CCD camera (Roper Scientific), Olympus 100 × 1.45 N.A., and Zeiss 100 × 1.4 N.A. objective lens. The acquisition was controlled by Metamorph (Molecular Devices). The exposure time was 100 ms unless specially indicated. Three types of lasers were used: a 442 nm solid state laser, a 488 nm and 514 nm argon gas laser, and a 568 nm and 647 nm red krypton and argon gas laser. TIRF images were analyzed by Image Pro Plus (Media Cybernetics), Image J (NIH, U.S.), or Matlab (Mathworks) software as indicated. Before analysis, images were split, aligned, background subtracted, and corrected for spectral bleedthrough using either Image ProPlus or Matlab software. Imaging of BCR, antigen, and pSyk microclusters by TIRFM were as recently described (Depoil et al., 2008; Tolar et al., 2009a) and detailed as Supplemental Information.

Single-Particle Tracking and Analysis

J558L cells were incubated with 1 nM of Alexa 568-anti-IgG as described (Tolar et al., 2009a). The acquisition and analyses of single BCR molecule TIRF images were as described (Tolar et al., 2009a). Briefly, a subregion of roughly 100 × 100 pixels of the available area of the EMCCD chip (512 × 512 pixels) was used to achieve an exposure time of 35 ms per frame. Single BCR molecules were captured on 300 frames in a time course of 10 s in streamline acquisition mode, the time resolution of which was found to be sufficient to reliably track the single molecule BCRs as reported (Tolar et al., 2009a). Single-molecule tracking was performed using Matlab (Mathworks) code based on available positional fitting and tracking algorithms (Crocker and Grier, 1996; Douglass and Vale, 2008). Mean square displacements (MSD) and short-range diffusion coefficients for each BCR molecule trajectories (D_0, based on time intervals of 35-140 ms) were calculated from positional coordinates as described (Douglass and Vale, 2008). The MSD plot was mathematically fitted into a confined diffusion model by an exponential function to acquire the size of the confinement microdomain.

Analysis of Fluorescence Intensities and Sizes of the BCR and Antigen Microclusters

Precise 2D positions and integrated FI of the BCR or antigen microclusters in time-lapse TIRF images were obtained by means of least-squares fitting of a 2D Gaussian function as below to each of the 2D FI profiles at each time point (Holtzer et al., 2007).

$$f(x,y) = z_0 + I\frac{4\ln 2}{\pi\sigma_f^2}e^{-\left[4\ln 2\left(\frac{(x-x_c)^2}{\sigma_f^2/r^2}+\frac{(y-y_c)^2}{\sigma_f^2 r^2}\right)\right]}$$

For each microcluster the fit yields "personalized" 2D Gaussian functions to mathematically describe the point spreading of the microcluster in each image at each time point. The "personalized" 2D Gaussian functions give the parameters of local background FI (z_0), position (x_c, y_c), integrated FI (I), and generalized full width at half maximum peak height (FWHM, σ_x, σ_y) of the intensity distribution in x and y direction, respectively, as described in detail (Liu et al., 2010). Only microclusters that were successfully tracked for at least 10 steps and only the first 60 steps (120 s) of each track from J558L microclusters were selected for analysis. This selection was necessary in order to avoid tracking and Gaussian fitting errors, both of which arise from spots merging and overlapping at later stages of the observed processes. Arithmetic means and standard errors of the FI or FWHM values of individual microcluster were calculated for all selected spots present in one frame and plotted versus time. Values belonging to the same track were normalized to the first position. The statistical test used to compare the kinetics of microcluster growth is as described (Baldwin et al., 2007; Elso et al., 2004; Hammarlund et al., 2003) or through online server (http://bioinf.wehi.edu.au/software/compareCurves/index.html).

SUPPLEMENTAL INFORMATION

Supplemental information includes Supplemental Experimental Procedures, seven Supplemental Figures and seven supplemental movies and can be found online at doi:10.1016/j.immuni.2010.06.006.

ACKNOWLEDGMENTS

We thank Dr. Garnett Kelsoe, Duke University, Dr. Robert Brink, Garvan Institute of Medical Research of Australia, and Dr. Christopher C Goodnow, the Australian National University, for generously providing experimental materials, and as always, we thank Dr. Joseph Brzostowski for expert advice on imaging. We thank Bhaskar Upadhyaya for charactering the Igα-YFP Tg C57BL/6 mice. This work has been supported by the Intramural Research Program of the National Institutes of Health, National Institute of Allergy and Infectious Diseases.

Received: December 17, 2009
Revised: April 22, 2010
Accepted: June 2, 2010
Published online: June 17, 2010

REFERENCES

Allen, D., Simon, T., Sablitzky, F., Rajewsky, K., and Cumano, A. (1988). Antibody engineering for the analysis of affinity maturation of an anti-hapten response. EMBO J. *7*, 1995–2001.

Baldwin, T., Sakthianandeswaren, A., Curtis, J.M., Kumar, B., Smyth, G.K., Foote, S.J., and Handman, E. (2007). Wound healing response is a major contributor to the severity of cutaneous leishmaniasis in the ear model of infection. Parasite Immunol. *29*, 501–513.

Batista, F.D., and Harwood, N.E. (2009). The who, how and where of antigen presentation to B cells. Nat. Rev. Immunol. *9*, 15–27.

Crocker, J.C., and Grier, D.G. (1996). Methods of Digital Video Microscopy for Colloidal Studies. J. Colloid Interface Sci. *179*, 298–310.

Dal Porto, J.M., Haberman, A.M., Kelsoe, G., and Shlomchik, M.J. (2002). Very low affinity B cells form germinal centers, become memory B cells, and participate in secondary immune responses when higher affinity competition is reduced. J. Exp. Med. *195*, 1215–1221.

Davis, R.E., Ngo, V.N., Lenz, G., Tolar, P., Young, R., Romesser, P.B., Kohlhammer, H., Lamy, L., Zhao, H., Yang, Y., et al. (2010). Chronic active B cell receptor signaling in diffuse large B cell lymphoma. Nature *463*, 88–92.

Depoil, D., Fleire, S., Treanor, B.L., Weber, M., Harwood, N.E., Marchbank, K.L., Tybulewicz, V.L., and Batista, F.D. (2008). CD19 is essential for B cell activation by promoting B cell receptor-antigen microcluster formation in response to membrane-bound ligand. Nat. Immunol. *9*, 63–72.

Douglass, A.D., and Vale, R.D. (2008). Single-molecule imaging of fluorescent proteins. Methods Cell Biol. *85*, 113–125.

Elso, C.M., Roberts, L.J., Smyth, G.K., Thomson, R.J., Baldwin, T.M., Foote, S.J., and Handman, E. (2004). Leishmaniasis host response loci (lmr1-3) modify disease severity through a Th1/Th2-independent pathway. Genes Immun. *5*, 93–100. 10.1038/sj.gene.6364042.

Engels, N., König, L.M., Heemann, C., Lutz, J., Tsubata, T., Griep, S., Schrader, V., and Wienands, J. (2009). Recruitment of the cytoplasmic adaptor Grb2 to surface IgG and IgE provides antigen receptor-intrinsic costimulation to class-switched B cells. Nat. Immunol. *10*, 1018–1025.

Fleire, S.J., Goldman, J.P., Carrasco, Y.R., Weber, M., Bray, D., and Batista, F.D. (2006). B cell ligand discrimination through a spreading and contraction response. Science *312*, 738–741.

Hammarlund, E., Lewis, M.W., Hansen, S.G., Strelow, L.I., Nelson, J.A., Sexton, G.J., Hanifin, J.M., and Slifka, M.K. (2003). Duration of antiviral immunity after smallpox vaccination. Nat. Med. *9*, 1131–1137.

Harwood, N.E., and Batista, F.D. (2008). New insights into the early molecular events underlying B cell activation. Immunity *28*, 609–619.

Holtzer, L., Meckel, T., and Schmidt, T. (2007). Nanometric three-dimensional tracking of individual quantum dots in cells. Appl. Phys. Lett. *90*, 05902.

Horikawa, K., Martin, S.W., Pogue, S.L., Silver, K., Peng, K., Takatsu, K., and Goodnow, C.C. (2007). Enhancement and suppression of signaling by the conserved tail of IgG memory-type B cell antigen receptors. J. Exp. Med. *204*, 759–769.

Kaisho, T., Schwenk, F., and Rajewsky, K. (1997). The roles of gamma 1 heavy chain membrane expression and cytoplasmic tail in IgG1 responses. Science *276*, 412–415.

Liu, W., Meckel, T., Tolar, P., Sohn, H.W., and Pierce, S.K. (2010). Antigen affinity discrimination is an intrinsic function of the B cell receptor. J. Exp. Med. *207*, 1095–1111.

Martin, S.W., and Goodnow, C.C. (2002). Burst-enhancing role of the IgG membrane tail as a molecular determinant of memory. Nat. Immunol. *3*, 182–188.

McHeyzer-Williams, L.J., and McHeyzer-Williams, M.G. (2005). Antigen-specific memory B cell development. Annu. Rev. Immunol. *23*, 487–513.

Paus, D., Phan, T.G., Chan, T.D., Gardam, S., Basten, A., and Brink, R. (2006). Antigen recognition strength regulates the choice between extrafollicular plasma cell and germinal center B cell differentiation. J. Exp. Med. *203*, 1081–1091.

Phan, T.G., Paus, D., Chan, T.D., Turner, M.L., Nutt, S.L., Basten, A., and Brink, R. (2006). High affinity germinal center B cells are actively selected into the plasma cell compartment. J. Exp. Med. *203*, 2419–2424.

Reth, M. (1992). Antigen receptors on B lymphocytes. Annu. Rev. Immunol. *10*, 97–121.

Shih, T.A., Meffre, E., Roederer, M., and Nussenzweig, M.C. (2002a). Role of BCR affinity in T cell dependent antibody responses in vivo. Nat. Immunol. *3*, 570–575.

Shih, T.A., Roederer, M., and Nussenzweig, M.C. (2002b). Role of antigen receptor affinity in T cell-independent antibody responses in vivo. Nat. Immunol. *3*, 399–406.

Sohn, H.W., Tolar, P., Jin, T., and Pierce, S.K. (2006). Fluorescence resonance energy transfer in living cells reveals dynamic membrane changes in the initiation of B cell signaling. Proc. Natl. Acad. Sci. USA *103*, 8143–8148.

Sohn, H.W., Tolar, P., and Pierce, S.K. (2008). Membrane heterogeneities in the formation of B cell receptor-Lyn kinase microclusters and the immune synapse. J. Cell Biol. *182*, 367–379.

Takahashi, Y., Dutta, P.R., Cerasoli, D.M., and Kelsoe, G. (1998). In situ studies of the primary immune response to (4-hydroxy-3-nitrophenyl)acetyl. V. Affinity maturation develops in two stages of clonal selection. J. Exp. Med. *187*, 885–895.

Tolar, P., and Pierce, S.K. (2009). Change we can believe in–of the conformational type. Workshop on the Initiation of Antigen Receptor Signaling. EMBO Rep. *10*, 331–336.

Tolar, P., and Pierce, S.K. (2010). A conformation-induced oligomerization model for B cell receptor microclustering and signaling. Curr. Top. Microbiol. Immunol. *340*, 155–169.

Tolar, P., Sohn, H.W., and Pierce, S.K. (2005). The initiation of antigen-induced B cell antigen receptor signaling viewed in living cells by fluorescence resonance energy transfer. Nat. Immunol. *6*, 1168–1176.

Tolar, P., Sohn, H.W., and Pierce, S.K. (2008). Viewing the antigen-induced initiation of B-cell activation in living cells. Immunol. Rev. *221*, 64–76.

Tolar, P., Hanna, J., Krueger, P.D., and Pierce, S.K. (2009a). The constant region of the membrane immunoglobulin mediates B cell-receptor clustering and signaling in response to membrane antigens. Immunity *30*, 44–55.

Tolar, P., Sohn, H.W., Liu, W., and Pierce, S.K. (2009b). The molecular assembly and organization of signaling active B-cell receptor oligomers. Immunol. Rev. *232*, 34–41.

Treanor, B., Depoil, D., Gonzalez-Granja, A., Barral, P., Weber, M., Dushek, O., Bruckbauer, A., and Batista, F.D. (2010). The membrane skeleton controls diffusion dynamics and signaling through the B cell receptor. Immunity *32*, 187–199.

Waisman, A., Kraus, M., Seagal, J., Ghosh, S., Melamed, D., Song, J., Sasaki, Y., Classen, S., Lutz, C., Brombacher, F., et al. (2007). IgG1 B cell receptor signaling is inhibited by CD22 and promotes the development of B cells whose survival is less dependent on Ig alpha/beta. J. Exp. Med. *204*, 747–758.

Wakabayashi, C., Adachi, T., Wienands, J., and Tsubata, T. (2002). A distinct signaling pathway used by the IgG-containing B cell antigen receptor. Science *298*, 2392–2395.